

Article

Electrochemical Synthesis of Precursors of Al₂O₃-ZrO₂ Ceramic Stabilized with Cerium Oxide and Magnesium Aluminate

Alexander F. Dresvyannikov , Ekaterina V. Petrova  and Laysan I. Kashfrazeyeva

Kazan National Research Technological University, 420015 Kazan, Russia; katrin-vv@mail.ru (E.V.P.); kashfrazieva_lesea@mail.ru (L.I.K.)

* Correspondence: a.dresvyannikov@mail.ru

Abstract: This article presents a new approach to preparing the precursors of complex oxide systems Al₂O₃-ZrO₂-M_XO_Y (M = Mg, Ce). The approach is based on the electrogeneration and interaction of reagents with electrolyte components in a coaxial electrochemical reactor. The design of the electrolyzer provides the suspension homogenization due to the turbulence induced by the intensive hydrogen bubbles and electrolyte movement in opposite directions relative to the central electrode in a closed space. Hydrogen evolution leads to the mixing of the solution. The transfer of OH⁻ ions generated at the cathode into the electrolyte and interaction with metal ions (Zr, Al, Ce, Mg) leads to the formation of hydroxo-aqua complexes of these metals. They participate in the polycondensation reaction, forming polymerized hydroxides and oxyhydroxides, which are the basis of the primary particles. The process of hydroxylation of nanoparticle surface of the formed precursors of oxide systems stabilizes the dispersion and prevents particle aggregation. The stabilized tetragonal t-ZrO₂ was obtained by sintering the precursor of the synthesized oxide system at 1100 °C with the formation of an alumina phase (γ-Al₂O₃, or an aluminum–magnesium spinel MgAl₂O₄) with a low CeO₂ content (2–3 wt%).



Citation: Dresvyannikov, A.F.; Petrova, E.V.; Kashfrazeyeva, L.I. Electrochemical Synthesis of Precursors of Al₂O₃-ZrO₂ Ceramic Stabilized with Cerium Oxide and Magnesium Aluminate. *Inorganics* **2022**, *10*, 57. <https://doi.org/10.3390/inorganics10050057>

Academic Editor: Christian Julien

Received: 22 February 2022

Accepted: 18 April 2022

Published: 20 April 2022

Publisher's Note: MDPI stays neutral with regard to jurisdictional claims in published maps and institutional affiliations.



Copyright: © 2022 by the authors. Licensee MDPI, Basel, Switzerland. This article is an open access article distributed under the terms and conditions of the Creative Commons Attribution (CC BY) license (<https://creativecommons.org/licenses/by/4.0/>).

Keywords: alumina/zirconia/cerium composition; precursor; electrogeneration; anode dissolution; hydroxo-aqua complexes; primary particles; sintering; phase content; tetragonal t-ZrO₂

1. Introduction

There is a growing industrial demand for Al₂O₃-ZrO₂ ceramic materials due to their high static bending strength, shear modulus and Poisson's ratio. The presence of a tetragonal phase of zirconium dioxide, partially stabilized with yttrium, cerium oxides or oxides of other elements (REE, Ca, Mg), provides these materials with improved properties such as hardness, crack and wear resistance, refractoriness, and inertness to chemically aggressive media. The ceramic properties depend on characteristics of initial powders, which are directly related to their synthesis method [1,2].

Traditionally, ceramic powders are obtained by mechanical grinding of initial oxides [3]. The main disadvantage of this method is the lack of constant control of grinding and mixing degree of components during the process.

Al₂O₃-ZrO₂ powders have also been developed by various chemical routes, such as the sol-gel method [4], hydrothermal synthesis [5], the coprecipitation method [6,7], and the solution combustion synthesis route [8]. Many contributions indicate that the key to synthesizing nano-sized Al₂O₃-ZrO₂ nanopowders is to prevent particle agglomeration during the formation of the precursors. However, the synthesis of Al₂O₃-ZrO₂ nanopowders is highly sensitive to all of the experimental factors. All of these factors can cause the agglomeration of Al₂O₃-ZrO₂ nanopowders in the coprecipitation process, eventually resulting in the formation of powders with poor dispersibility, large particle size, and wide particle size distribution [9,10].

To obtain homogeneous powder composition, liquid-phase synthesis methods (coprecipitation, sol-gel, hydrothermal and electrochemical methods) are used [11–19]. The

electrochemical method is one of the most reliable. It does not require special reagents and provides a high degree of homogenization of precursor particles of ceramic powders. This method allows us to control the process of reagents generation and coprecipitation by regulating electrical parameters.

Nevertheless, as far as we know, the reported studies on the influence of electrochemical methods on the physicochemical properties of $\text{Al}_2\text{O}_3\text{-ZrO}_2$ powders are still limited.

The aim of this work is to synthesize by an electrochemical method powders of the $\text{Al}_2\text{O}_3\text{-ZrO}_2\text{-CeO}_2$ composition, containing Mg_2AlO_4 spinel to increase the thermal stability of the ceramics. The main objective of this work is to study the possibility of using an approach based on the electrical generation of a part of the reagents and their interaction with electrolyte components in a coaxial electrolytic reactor to obtain precursors of complex oxide systems $\text{Al}_2\text{O}_3\text{-ZrO}_2\text{-M}_x\text{O}_y$ ($M = \text{Mg, Ce}$) and the estimation of physicochemical properties.

2. Results and Discussion

The electrolyzer configuration was chosen according to the symmetric picture of the electric field and a significant difference in the surfaces of cathode and anode. The anode surface area is 100 times as large as the cathode surface area. Therefore, the current density at the central cathode significantly exceeds the current density at the peripheral anode, which affects the process rate.

The electrochemical reactions on the electrodes increase natural convection due to changes in reagent concentrations near the electrode surfaces, as well as due to gas evolution and heating of the central electrode. The rate of gas evolution depends on electrochemical process conditions and electrolyzer geometry [20]. The higher the electric field strength and the magnitude of the charge, the greater the ponderomotive forces that detach the bubble from the electrode and make the dimension of bubbles smaller [21]. Gas bubbles move in the direction from the bottom to the top of the unit and cause reaction blend mixing [22].

The intense hydrogen evolution at the central electrode leads to the formation of hydrodynamic flows directed along the electrode, which ensures the transfer of reaction products to the cathode along a toroidal trajectory from the center to the peripheral anode (Figure 1).

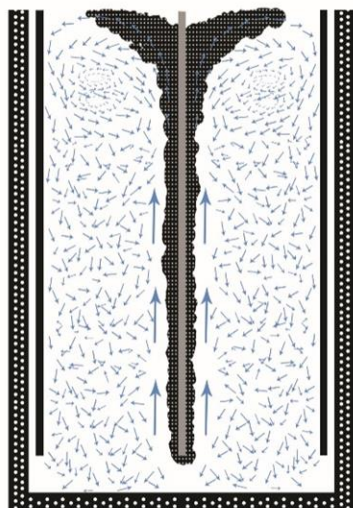
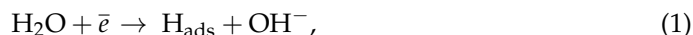


Figure 1. Hydrodynamic flows in a coaxial electrolyzer.

This allows the products of the cathodic reaction (OH^- ions, radicals, etc.) to reach the anode surface in a short time that prevents the aggregation of the formed particles. The process of alkalization in the electrolyzer takes less than a minute.

In alkaline solution, the discharge of water molecules proceeds according to the scheme [23]:



The hydrogen evolution overpotential decreases in the alkaline solution. It also decreases with increasing temperature under the influence of Joule heat during electrolysis.

The transfer of OH^- ions generated at the cathode into the electrolyte and interaction with metal ions (Zr, Al, Ce, Mg) leads to the formation of hydroxo aqua complexes of these metals. They participate in the polycondensation reaction, forming polymerized hydroxides and oxyhydroxides, which are the basis of the primary particles.

In the anodic dissolution of aluminum, cations Al^{3+} and $\text{Al}(\text{OH})_2^+$ are formed. They are transformed into $\text{Al}(\text{OH})_3$ and then polymerized in the form of $\text{Al}_n(\text{OH})_{3n}$ at a pH 8 [24].

The process of anodic dissolution of aluminum and the interaction of hydroxyl ions with metal ions (electrically generated and presented in the electrolyte) lead to the formation of primary particles of highly dispersed oxide precursors of these metals in the volume of the electrochemical reactor. The current efficiency is associated with the presence of cations of metals (Zr^{4+} , Ce^{4+} and Mg^{2+}) in electrolyte, which intensify the anodic dissolution of aluminum (Table 1). A significant excess (>100%) of the current efficiency is explained by the influence of metal cations on the anodic dissolution of aluminum and the phenomenon of a negative difference effect.

Table 1. Grade and composition of Al_2O_3 - ZrO_2 .

Sample Designation	Content, (wt%)				ξ , mV	Current Efficiency, %
	Al_2O_3	ZrO_2	MgO	CeO_2		
10 wt% ZrO_2 - Al_2O_3 - CeO_2	87.14	10.7	-	2.15	4.8	124
5 wt% ZrO_2 - Al_2O_3 - MgO - CeO_2	90.15	4.06	3.07	2.71	37.5	115
1 wt% ZrO_2 - Al_2O_3 - MgO - CeO_2	94.03	0.94	2.73	2.3	13.4	138

Polarization measurements were used to assess the effect of the ionic composition of the solution on the anodic dissolution process. The kinetics of anodic dissolution of aluminum depending on the electrolyte composition was studied. Chloride ions are the strongest activators of anodic dissolution of passivated metals. They promote the transformation of the surface oxide layer and dissolution of aluminum [25]. The joint presence of zirconium, magnesium, cerium, nitrate, and chloride ions in the electrolyte intensifies the process of metal dissolution. This was proved by the characters of the anodic polarization curves (Figure 2).

The suspension stability to the aggregation is characterized by the values of the ξ -potential and depends on the size of particles, their chemical and phase composition, and the nature of the dispersion medium.

The particle stability of the synthesized precursors of oxide systems decreases over time as a result of hydroxylation of the surface of these particles due to the continuous generation of OH^- ions at the cathode [26]. Zr (IV), Mg (II) and Ce (IV) ions also affect the behavior of the disperse system, reducing the value of the ξ -potential with time, which indicates the metastability of the obtained systems (Table 2).

Table 2. Data of differential scanning calorimetry.

Sample Designation	Temperature Range (T_{max}), °C				Total Weight Loss, (wt%)
	Weight Loss, (wt%).				
10 wt% ZrO_2 - Al_2O_3 - CeO_2	30–190 (81)	190–310 (271)	310–500 (–)	500–1000 (–)	34.38
	12.40	14.54	4.82	2.62	
1 wt% ZrO_2 - Al_2O_3 - MgO - CeO_2	30–180 (97)	180–300 (217;255)	300–500 (346)	500–1000 (–)	31.94
	13.10	8.57	7.85	2.42	

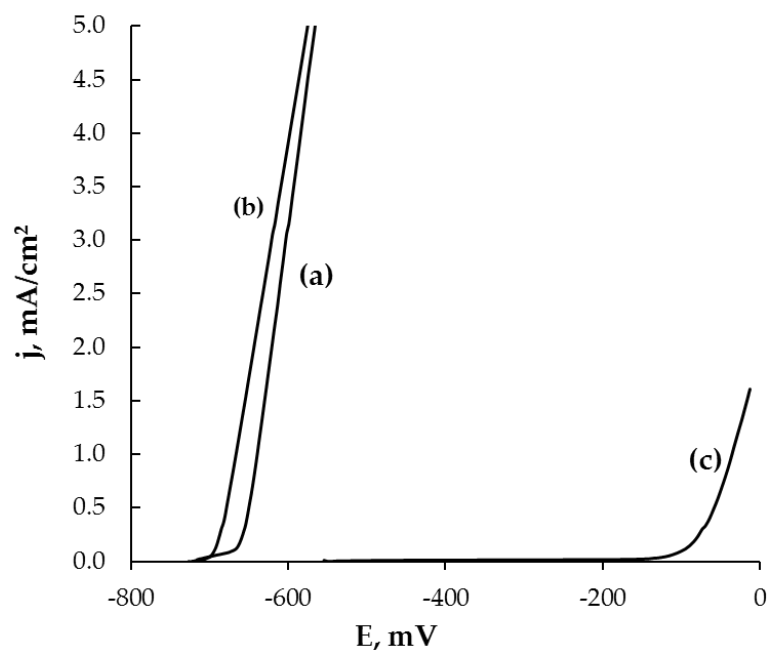


Figure 2. Anode polarization curves of aluminum electrode in solutions: (a) 0.5 M NaCl + 0.045 M $Zr(NO_3)_2$ + 0.006 M $Ce(NO_3)_4$; (b) 0.5 M NaCl + 0.030 $Zr(NO_3)_2$ + 0.050 M $Mg(NO_3)_2$ + 0.006 M $Ce(NO_3)_4$; (c) 0.1 M NaCl + 0.030 $Zr(NO_3)_2$ + 0.050 M $Mg(NO_3)_2$ + 0.006 M $Ce(NO_3)_4$.

An excess of OH^- ions coming from the cathode gradually leads to hydroxylation of the particle surface. The simultaneous presence of metal ions with different valence in the electrolyte, differing in their coagulating ability, may lead to the adsorption of counter-ions in superequivalent amounts. The combination of these factors leads to the propensity of particles to change the ξ -potential. For oxide system No. 1, the proposed ionic composition contributes to the formation of the most stable particles. With an increase in the concentration of chloride ions up to 0.5 M in a four-component electrolyte and after two hours of treatment of the suspension in the electric field, a fourfold decrease in the ξ -potential is observed. It is associated with an increase in the content of hydrated polyions according to the Faraday law.

Figure 3 presents SEM-images of the synthesized samples. The introduction of magnesium and the increase of anodic current density result in a decrease in the size of subindividuals aggregated into larger formations.

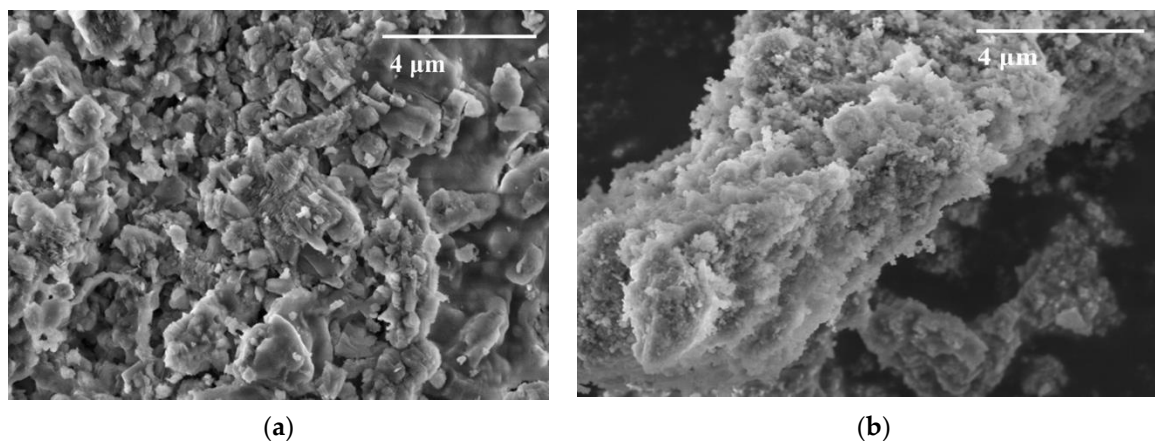


Figure 3. SEM image samples: (a) 10 wt% ZrO_2 - Al_2O_3 - CeO_2 ; (b) 1 wt% ZrO_2 - Al_2O_3 MgO - CeO_2 .

The TGA data (Figure 4) show that the process of dehydration proceeds gradually and continuously due to the interaction of the surface of precursor particles of complex oxide systems with electrochemically generated OH^- ions.

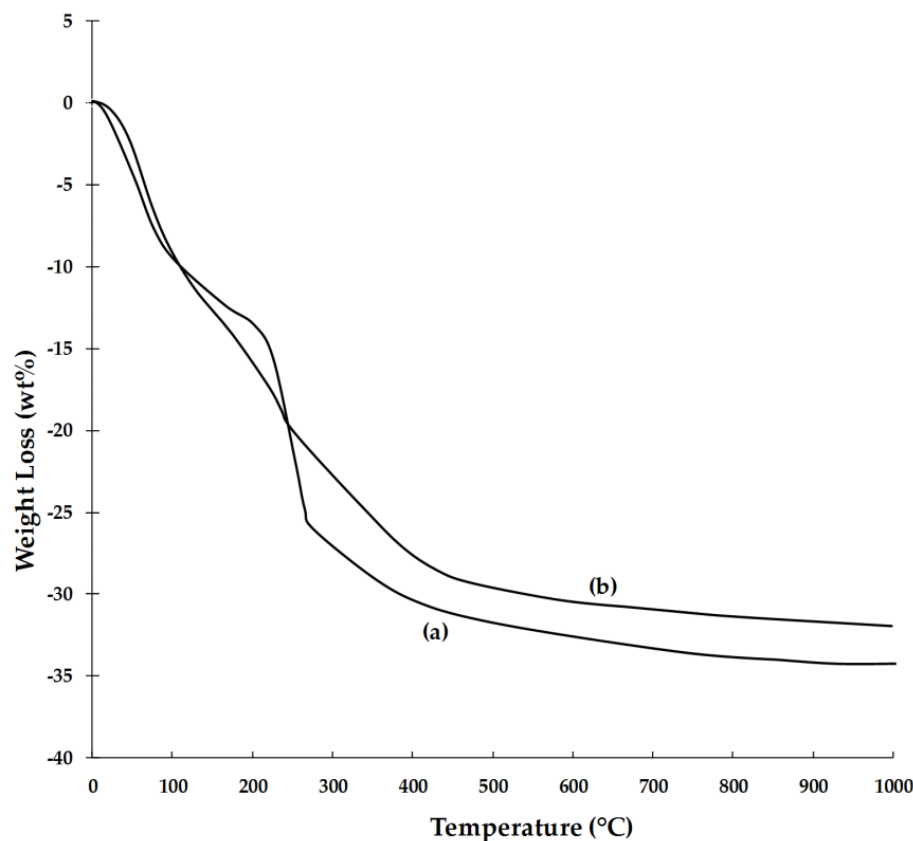


Figure 4. TGA curve samples: (a) 10 wt% $\text{ZrO}_2\text{-Al}_2\text{O}_3\text{-CeO}_2$; (b) 1 wt% $\text{ZrO}_2\text{-Al}_2\text{O}_3\text{ MgO-CeO}_2$.

Desorption of physically bound water (adsorbed and crystallization) corresponds to the first endothermic effect in the temperature range 30–180 °C (Table 2). The second endothermic effect in the temperature range 180–310 °C is associated with the removal of coordinated water from the bayerite structure, and the formation of two phases: boehmite and low-temperature aluminum oxide ($\eta\text{-Al}_2\text{O}_3$). In this temperature range, dehydration of zirconium hydroxide occurs with the formation of cubic zirconium dioxide.

The high-temperature endothermic effect at 300–500 °C characterizes the removal of water from the boehmite structure and the formation of $\gamma\text{-Al}_2\text{O}_3$. A phase transformation of cubic zirconium dioxide into tetragonal structure was observed in the same temperature ranges. The third low-intensity peak on the DSC curves at a temperature of about 500–1000 °C is an additive effect caused by the dehydration of pseudoboehmite and further phase transition of zirconium dioxide.

The total weight loss is of the same order of magnitude and is most likely associated with the removal of chemisorbed water. In any case, the proposed approach may be used to obtain an oxide system consisting of a stabilized t- ZrO_2 , an aluminum-containing $\gamma\text{-Al}_2\text{O}_3$ phase, or an aluminum–magnesium spinel MgAl_2O_4 with a low (2–3 wt%) CeO_2 content, which is confirmed by X-ray phase analysis data (Figure 5).

The experimental results prove that the proposed approach allows us to obtain complex oxide systems based on the $\text{Al}_2\text{O}_3\text{-ZrO}_2$ binary system, characterized by the presence of a tetragonal zirconium dioxide phase in them, which is stable over a wide temperature range.

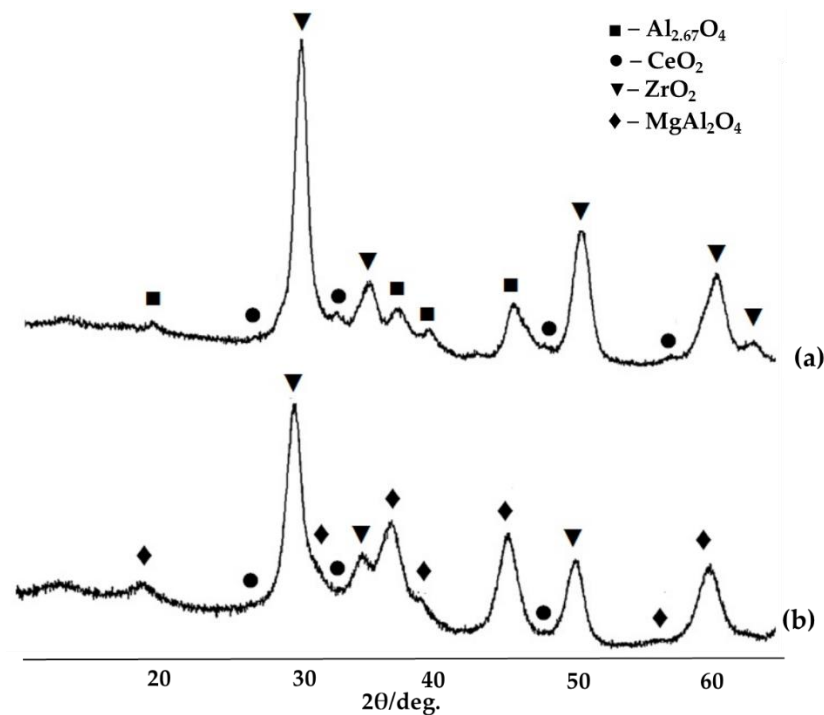
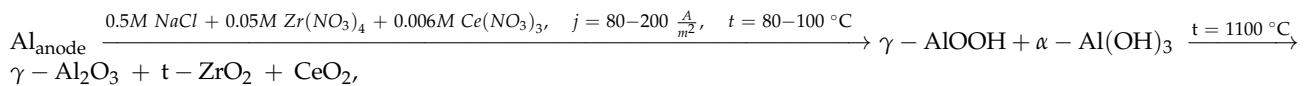


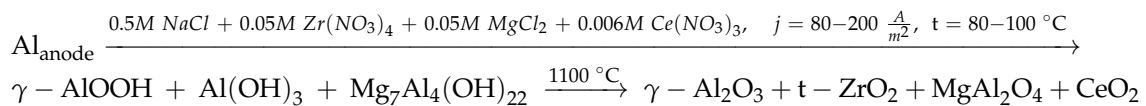
Figure 5. XRD patterns: (a) 10 wt% ZrO₂-Al₂O₃-CeO₂; (b) 1 wt% ZrO₂-Al₂O₃ MgO-CeO₂.

The transformation chains are presented below.

For Al₂O₃-ZrO₂-CeO₂ system:



and for the system Al₂O₃-ZrO₂-MgO-CeO₂:



The transformation of ionic forms and their transition to heterogeneous phases for reagent electrogeneration using a soluble anode include the formation of polynuclear aquahydroxocomplexes, which are precursors of primary particles (PM) of oxide precursors [27]. The interaction of electrogenerated OH ions and hydrated metal ions leads to the formation of aqua hydroxo complexes. In addition, polynuclear complexes are formed which participate in polycondensation processes [26]. The growth of polymerized ions leads to the formation of PM. They form amorphous structures with their subsequent crystallization.

3. Materials and Methods

The synthesis of precursors of the oxide systems was performed in a coaxial electrolyzer, similar to a cylindrical capacitor with a highly inhomogeneous electric field, where the cathode was a rod of high-alloy steel 316 L, and the anode was made of aluminum with a purity 99.7%. The solution of sodium chloride with a concentration of 0.5 mol/L was used as an electrolyte. The weight fraction of ZrO₂, CeO₂, and MgO in the alumina system was controlled by varying the concentration of an ion modifier in the electrolyte. The process was performed at an anodic current density of 80–200 A/m² followed by keeping the precipitate in an electrolyte solution for 48 h.

The sediment was centrifuged, washed with bidistillate until neutral reaction, dried at 80 °C to constant weight, and heated at 1100 °C for two hours.

The phase composition of the sample was analyzed by a D2 PHASER X-ray diffractometer (Bruker, $\text{CoK}\alpha$ -radiation, $\lambda = 1.78892 \text{ \AA}$). Crystalline phases were identified using the PDF-2 database.

X-ray fluorescence analysis was carried out using a Bruker S2 PICOFOX spectrometer. A Mastersizer 2000 laser analyzer, Malvern was used to determine the particle size distribution.

Thermal analysis was performed using an STA 6000 synchronous thermal analyzer (PerkinElmer). The sample heating was carried out in a corundum crucible in air in the temperature range of 30–1000 °C with a change rate of 10 °C/ min.

4. Conclusions

A new approach to preparing precursors of complex oxide systems $\text{Al}_2\text{O}_3\text{-ZrO}_2\text{-M}_x\text{O}_y$ ($M = \text{Mg, Ce}$) was proposed. It is based on the electrogeneration and interaction of reagents with electrolyte components under conditions of a specific hydrodynamic regime in a coaxial electrolytic reactor with electrodes which differ significantly in areas. The design of the electrolyzer provides homogenization of the suspension due to turbulence resulting from the intensive movement of gas and electrolyte bubbles in opposite directions relative to the central electrode in a closed space.

It was found that the current efficiency of the anodic process exceeds 100% due to the difference effect and the influence of the ionic composition of the electrolyte on the anodic dissolution of aluminum. The intensification of the anodic dissolution by increasing the NaCl results in an approximately 1.8-fold increase in the average particle size. The injection of Mg^{2+} ions into the electrolyte leads to a 1.5-fold decrease in the average particle size as well as to the formation of a disperse system with a more uniform particle size distribution.

The injection of the Zr^{4+} , Mg^{2+} , Ce^{4+} cations, and the NO_3^- anion into the electrolyte leads to the change in the value of the ξ -potential and indicates the metastability of the obtained systems. This approach is distinguished by the internal electrochemical generation of a part of the reagents and stabilization of the dispersions as a result of continuous hydroxylation of the surface of the formed precursors of oxide system nanoparticles, preventing particle aggregation. The method can be used to obtain oxide systems consisting of a stabilized t- ZrO_2 , an aluminum-containing phase ($\gamma\text{-Al}_2\text{O}_3$, or an aluminum–magnesium spinel MgAl_2O_4) with a low CeO_2 content (2–3 wt%).

Author Contributions: This work is the collaborative development of all the authors. Conceptualization, A.F.D. and E.V.P.; methodology, A.F.D. and E.V.P.; software, L.I.K.; validation, A.F.D. and E.V.P.; formal analysis, L.I.K.; investigation, A.F.D., E.V.P. and L.I.K.; resources, A.F.D.; data curation, A.F.D. and E.V.P.; writing—original draft preparation, E.V.P. and L.I.K.; writing—review and editing, A.F.D.; supervision, A.F.D. and E.V.P. All authors have read and agreed to the published version of the manuscript.

Funding: This research was funded by the Ministry of Science and Higher Education of the Russian Federation, grant number 075-00315-20-01.

Informed Consent Statement: Consent was obtained from all study participants.

Data Availability Statement: Not applicable.

Acknowledgments: The study was carried out using the equipment of the Center for Collective Use “Nanomaterials and Nanotechnology” of the Kazan National Research Technological University.

Conflicts of Interest: The authors declare no conflict of interests.

References

1. Chevalier, J.; Liens, A.; Reviron, H.; Zhang, F.; Reynaud, P.; Douillard, T.; Preiss, L.; Sergo, V.; Lughi, V.; Swain, M.; et al. Forty years after the promise of «ceramic steel?»: Zirconia-based composites with a metal-like mechanical behavior. *J. Am. Ceram. Soc.* **2020**, *103*, 1482–1513. [[CrossRef](#)]
2. Fu, L.-S.; Chen, G.-Q.; Fu, X.-S.; Zhou, W.-L. Insights into the ternary eutectic microstructure formed in intercolony regions in $\text{Al}_2\text{O}_3\text{-ZrO}_2(\text{Y}_2\text{O}_3)$ system. *J. Am. Ceram. Soc.* **2018**, *102*, 498–507. [[CrossRef](#)]

3. Kimura, Y.; Kushi, T.; Unemoto, A.; Amezawa, K.; Kawada, T. Influence of aging on mechanical properties of yttria-doped zirconia. *Ceramics* **2018**, *1*, 287–303. [[CrossRef](#)]
4. Lamas, D.G.; Lascalea, G.E.; Juarez, R.E.; Djurado, E.; Pérez, L.; de Reca, N.E.W. Metastable forms of the tetragonal phase incompositionally homogeneous, nanocrystalline zirconia–ceria powders synthesised by gel-combustion. *J. Mater. Chem.* **2003**, *13*, 904–910. [[CrossRef](#)]
5. Herrmann, M.; Seipel, B.; Schilm, J.; Nickel, K.G.; Michael, G.; Krell, A. Hydrothermal corrosion of zirconia-toughened alumina (ZTA) at 200 °C. *J. Eur. Ceram. Soc.* **2005**, *25*, 1805–1812. [[CrossRef](#)]
6. Chuang, C.-C.; Hsiang, H.-I.; Hwang, J.S.; Wang, T.S. Synthesis and characterization of Al₂O₃-Ce_{0.5}Zr_{0.5}O₂ powders prepared by chemical coprecipitation method. *J. Alloy. Compd.* **2009**, *470*, 387–392. [[CrossRef](#)]
7. Liu, G.; Xie, Z.; Wu, Y. Effectively inhibiting abnormal grain growth of alumina in ZTA with low-content fine-sized ZrO₂ inclusions introduced by infiltration and in situ precipitation. *J. Am. Ceram. Soc.* **2010**, *93*, 4001–4004. [[CrossRef](#)]
8. Manfredi, D.G.; Ambrosio, E.P.; Biamino, S.; Badini, C.F.; Fino, P. Al₂O₃-ZrO₂ nanocomposites produced by solution combustion synthesis followed by ultrasonic milling. *J. Ceram. Process. Res.* **2011**, *12*, 207–211. [[CrossRef](#)]
9. Huang, B.; Ren, R.; Zhang, Z.; Zheng, S. The improvement of dispersibility of YIG precursor prepared via chemical coprecipitation. *J. Alloy. Compd.* **2013**, *558*, 56–61. [[CrossRef](#)]
10. Patil, S.B.; Jena, A.K.; Bhargava, P. Influence of ethanol amount during washing on deagglomeration of co-precipitated calcined nanocrystalline 3YSZ powders. *Int. J. Appl. Ceram. Technol.* **2013**, *10*, E247–E257. [[CrossRef](#)]
11. Yu, W.; Zheng, Y.; Yu, Y.; Liu, X.; Yuan, Y. The microstructure, formation mechanism and sintering characteristics of Al₂O₃/ZrO₂ supersaturated solid solution powders. *Ceram. Int.* **2021**, *47*, 25264–25273. [[CrossRef](#)]
12. Promakhov, V.; Zhukov, A.; Dubkova, Y.; Zhukov, I.; Kovalchuk, S.; Zhukova, T.; Olisov, A.V.; Klimenko, V.A.; Savkina, N. Structure and properties of ZrO₂-20%Al₂O₃ ceramic composites obtained using additive technologies. *Materials* **2018**, *11*, 2361. [[CrossRef](#)] [[PubMed](#)]
13. Therese, G.H.A.; Kamath, P.V. Electrochemical synthesis of metal oxides and hydroxides. *Chem. Mater.* **2000**, *12*, 1195–1204. [[CrossRef](#)]
14. Guo, W.-M.; Zeng, L.-Y.; Wu, L.-X.; Wang, H.-J.; Sun, S.-K.; Lin, H.-T.; Wu, S.-H.; Wang, C.-Y. Effect of CeO₂ and Al₂O₃ contents on Ce-ZrO₂/Al₂O₃ composites. *J. Am. Ceram. Soc.* **2018**, *101*, 2066–2073. [[CrossRef](#)]
15. Abi, C.B.; Emrullahoglu, O.F.; Said, G. Microstructure and mechanical properties of MgO-stabilized ZrO₂-Al₂O₃ dental composites. *J. Mech. Behav. Biomed. Mater.* **2013**, *18*, 123–131. [[CrossRef](#)]
16. Rejab, N.A.; Azhar, A.Z.A.; Kian, K.S.; Ratnam, M.M.; Ahmad, Z.A. Effects of MgO addition on the phase, mechanical properties, and microstructure of zirconia-toughened alumina added with CeO₂ (ZTA-CeO₂) ceramic composite. *Mater. Sci. Eng. A* **2014**, *595*, 18–24. [[CrossRef](#)]
17. Mitra, N.K.; Das Supratim Maitra, S.; Sengupta, U.; Basumajumdar, A. Effect of CeO₂ on the sintering behaviour of zirconia-alumina composite. *Ceram. Int.* **2002**, *28*, 827–833. [[CrossRef](#)]
18. Koltsov, I.; Smalc-Koziorowska, J.; Przeźniak-Welenc, M.; Małysa, M.; Kimmel, G.; McGlynn, J.; Ganin, A.; Stelmakh, S. Mechanism of reduced sintering temperature of Al₂O₃-ZrO₂ nanocomposites obtained by microwave hydrothermal synthesis. *Materials* **2018**, *11*, 829. [[CrossRef](#)]
19. Hu, J.; Tian, X.; Hu, C.; Luo, Y.; Peng, H.; Luo, J. Preparation of Al₂O₃-ZrO₂ composite powder by co-precipitation method in an alcohol-water solution and its sintering behavior. *J. Ceram. Process. Res.* **2016**, *17*, 1181–1187.
20. Mata, M.D.; Aldasb, K.; Ilegbusi, O.J. A two-phase flow model for hydrogen evolution in an electrochemical cell. *Int. J. Hydrog. Energy* **2004**, *29*, 1015–1023. [[CrossRef](#)]
21. Bideau, D.; Mandin, P.; Benbouzid, M. Eulerian two-fluid model of alkaline water electrolysis for hydrogen production. *Energies* **2020**, *13*, 3394. [[CrossRef](#)]
22. Kantarci, N.; Borak, F.; Ulgen, K.O. Bubble column reactors. *Process Biochem.* **2005**, *40*, 2263–2283. [[CrossRef](#)]
23. Ota, K.I.; Kreysa, G.; Savinell, R.F. (Eds.) *Encyclopedia of Applied Electrochemistry*; Springer: New York, NY, USA, 2014.
24. Mansouri, K.; Ibrik, K.; Bensalah, N.; Abdel-Wahab, A. Anodic dissolution of pure aluminum during electrocoagulation process: Influence of supporting electrolyte, initial pH, and current density. *Ind. Eng. Chem. Res.* **2011**, *50*, 13362–13372. [[CrossRef](#)]
25. Guseva, O.; Schmutz, P.; Suter, T.; Trzebiatowsky, O. Modelling of anodic dissolution of pure aluminum in sodium chloride. *Electrochim. Acta* **2009**, *54*, 4514–4524. [[CrossRef](#)]
26. Petrova, E.V.; Dresvyannikov, A.F.; Khairullina, A.I.; Mezhevich, Z.V. Physicochemical properties of alumina synthesized with electrogenerated reagents. *Russ. J. Phys. Chem. A* **2019**, *93*, 1399–1405. [[CrossRef](#)]
27. Sakuma, T. Phase Transformation and microstructure of partially-stabilized zirconia. *Trans. Jpn. Inst. Met.* **1988**, *29*, 879–893. [[CrossRef](#)]